doi:10.1088/2053-1591/3/12/126502

First-principles study of transition metal carbides

Damien Connétable

CIRIMAT UMR 5085, CNRS-INP-UPS, ENSIACET 4, allée Émile Monso, BP 44362, F-31030 Toulouse Cedex 4, France

E-mail: damien.connetable@ensiacet.fr

Keywords: DFT, carbides, transition metals, alloys, elasticity, vibrational properties

Abstract

This study investigates the physical properties of transition metal carbides compounds associated with the Nb–C, Ti–C, Mo–C and W–C alloys systems using first-principles calculations. The ground-state properties (lattice parameters, cohesive energies and magnetism) were analyzed and compared to the experimental and theoretical literature. The simulations are in excellent agreement with experimental findings concerning atomic positions and structures. Elastic properties, computed using a finite-differences approach, are then discussed in detail. To complete the work, their lattice dynamics properties (phonon spectra) were investigated. These results serve to establish that some structures, which are mechanically stable, are dynamically unstable.

1. Introduction

Carbide compounds belong to a class of systems that are often used to harden solid solutions or for their intrinsic high mechanical properties and high melting point temperatures. However, their properties are rarely investigated from both an experimental and a theoretical standpoint. In comparison, transition metal nitrides, which belong to another prominent class of materials that also exhibits high chemical stability and hardness, have already been studied widely by means of first-principles calculations [1–3].

In nickel super-alloys and in titanium alloys, which are composed of many types of species, many precipitates are always present, carbides in particular. For instance, nickel-based super-alloys are materials capable of maintaining their high room-temperature mechanical properties even at elevated temperatures [4–6]. This ability is mainly attributed to the large number of metallic elements dissolved in the fcc Ni-matrix, which contribute to the mechanical properties by different strengthening mechanisms [5, 6]. One of them being the solid solution strengthening due to lattice distortions and alloying interference in lattice periodicity [5]. The strong reaction of alloying elements with carbon leading to carbides formation is used to strengthen by controlling grain size during elaboration processes, or enhancing high temperature mechanical properties by reducing grain boundary slip [5–7]. In titanium alloys, TiC structures can be found on the surface, which hardens the interface, but when formed within the matrix they reduce their mechanical properties. Furthermore, in alloys, when the carbon content, introduced by usage or manufacturing processes, is too high, it can precipitate and form many types of structures depending on the alloyed species. The physical properties of such structures are often poorly known even though they can significantly alter the properties of the matrix.

To understand the mechanical properties but also in the spirit of improving current and future materials, studying the main properties of these compounds is a modern way to design and predict structures. First-principles calculations can therefore be used to provide such information. Polycrystalline properties and simulations should include realistic properties, sometimes experimentally unreachable. For instance, elastic constants, Debye temperatures and formation energies can help to improve such macroscopic models. In the case of transition metal carbides, there has been little work dealing with their ground-states properties. These works focus mainly on electronic properties and some of them on elastic properties (in the case of Nb–C systems). Nevertheless, there are no comprehensive studies comparing and summarizing the elastic and vibrational properties of these compounds. The aim of the present paper is to bring an exhaustive overview of these properties of transition metal carbides.

Among the transition metal species, nickel does not form intermediate stable compounds with carbon [8], contrary to W, Mo, Nb and Ti species. We thus focused our attention on these four carbides systems: W–C, Mo–C, Nb–C and Ti–C alloys. We have put an on systems present in the phase diagrams, where identical crystallographic structures can be observed. Some of them were already investigated from their superconductivity properties, in particular the cF8 cubic structure, see discussion by Isaev [9]. In the following, we focus on ground state properties such as formation energies and lattice parameters, on elastic properties and finally on vibrational properties.

The remainder of this paper is organized into four sections. In section 2, we present the theoretical framework in which the structures were studied. We then present (section 3) ground state properties (lattice parameters, formation energies and atomic positions) of carbides X–C (X = Nb, Ti, W and Mo). Our results are discussed in the light of phase diagrams and experimental data. In section 4, the single-crystal elastic properties are presented and compared to the literature. To conclude (section 5), we will discuss their vibrational properties.

2. Computational details

The present calculations were performed based on the density functional theory (DFT), using the Vienna *ab-initio* simulation program (VASP) [10]. Calculations were done with projector augmented waves pseudo-potentials (PAW [11]), with a cut-off energy of 600 eV. The Perdew–Burke–Ernzerhof (PBE) [12] exchange and correlation functional within its spin-polarized version was used. To compute formation energies, elastic constants (using finite differences [13]) and crystal vibrations, integration over the Brillouin zone was carried out on dense meshes of k-points, approximately 10 000 k-points per atoms.

The inter-atomic force constants (IFCs) were calculated displacing only non-equivalent atoms along non-equivalent directions according to the symmetries of the system. The *phonopy* package [14] was used to generate finite displacements according to the symmetry of each structures, and it was then used to analyze and plot vibrational properties (phonon dispersion curves and density of states). For the calculation of IFCs, a super-cell approach was used, the lattice parameters of super-cells were taken larger than 10 Å, which corresponds to 1–4 primitive cells in each direction, depending on the size of the primitive cell.

3. Equilibrium properties

3.1. Nb–C alloys

We first put an emphasis on Nb–C compounds mainly taking account structures of the phase diagram. Seven binaries structures are referenced in this phase diagram, as pointed out by Smith *et al* [15]: NbC-cF8, NbC-hP2, Nb_4C_3-hR20, Nb_6C_5-mC22, α- β- and γ-Nb_2C.

One has a cubic symmetry: NbC-cF8 (NaCl-like structure, $Fm\bar{3}m$, space group *225*) where Nb atoms are in the *4b* sublattice (1/2, 1/2, 1/2), in Wyckoff notation, and C atoms are in the *4a* (0, 0, 0) sites (an fcc structure were octahedral sites are filled).

α-Nb_2C is an orthorhombic compound, considered by Smith as a meta stable structure at low temperature. In α-Nb_2C (*Pmcn*, *62*), all atoms (three non-equivalent sublattices) have the same Wyckoff positions: *4c* (x, 1/4, z). We found $x = 0.9907$, $z = 0.3751$ for C atoms, $x = 0.7540$, $z = 0.5455$ and $x = 0.2648$, $z = 0.7034$ for Nb atoms. These optimized positions are in excellent agreement with experimental positions, see [15].

There are also four hexagonal phases:

(i) NbC-hP2 (CW prototype, *187*), where C atoms are in *1f* (2/3, 1/3, 1/2) and Nb in *1a* (0, 0, 0): Nb atoms are at the corner of the hexagons and C atoms fill half of the interstitial sites of the hexagonal structure;

(ii) A high-temperature hexagonal structure (above 2500 °C): γ-Nb_2C hP3, (W_2C prototype, *164*), where C atoms are in *2a* (0, 0, 0) and Nb in *2d* (1/3, 2/3, $z = 0.2504$). Smith described it as an L'3 structure, where C atoms are randomly distributed on interstitial sites. In the ideal system, $z = 0.25$, but here, there is only one C atom on the 2*a* site.

(iii) β-Nb_2C hP9 (ϵ-Fe_2N, $P\bar{3}1m$, 162) observed at intermediate temperatures (800 °C–2500 °C). C atoms are located in the *1a* (0, 0, 0) and *2d* (1/3, 2/3, 1/2) sub-lattices, and Nb atoms in *6k* (x, 0, z). x and z were found equal to 0.3372 and 0.2498, respectively, experimental values are equal to $x \simeq 0.333$ and $z \simeq 0.25$.

(iv) Nb_4C_3-hR20 (V_4C_3, $R\bar{3}m$, 166), where Nb atoms are located in two *6c* positions (0, 0, z), where $z = 0.1205$ and 0.2920, and where 9 C atoms should be put in 12 sites of 3 sub-lattices: *3a* (0, 0, 0), *3b* (0, 0, 1/2) and *6c*

Table 1. The formation energies (E_f, in meV atom^{-1}), the lattice parameters of Nb–C alloys (Å): comparison with literature.

System		a_o	b_o	c_o	β (°)	E_f
C	cF8	3.573	—	—	—	0
		3.567[a]	—	—	—	—
NbC	cF8	4.510	—	—	—	−529
		4.49[b]	—	—	—	−581[c]
		4.430[d]	—	—	—	—
		4.480[h]	—	—	—	−562[h]
		4.517[i]	—	—	—	—
		4.476[e]	—	—	—	—
NbC	hP12	3.175	—	15.753	—	−513
		3.115[h]	—	—	—	−557[c]
NbC	hP2	3.071	—	2.894	—	−128
		3.05[c]	—	2.789[c]	—	−122[c]
Nb_4C_3	hR20	3.165	—	30.795	—	−461
		3.14[g]	—	30.1[g]	—	—
		3.145[h]	—	31.670[h]	—	−510[h]
Nb_6C_5	mC22	5.552	9.554	5.552	109.66	−611
		5.447[f]	9.435[f]	5.447[f]	109.47[f]	—
		5.489[h]	9.518[h]	5.484[h]	109.68[h]	−639[h]
α-Nb_2C	oP12	3.113	5.004	11.023	—	−515
		3.096[g]	4.968[g]	10.906[g]	—	—
		3.093[h]	4.985[h]	10.961[h]	—	−535[h]
β-Nb_2C	hP9	5.459	—	4.981	—	−505
		5.341[g]	—	4.968[g]	—	—
γ-Nb_2C	hP3	3.153	—	5.004	—	−500
		3.120[g]	—	4.957[g]	—	−505[c]
		3.115[h]	—	5.340[h]	—	−463[c]
Nb	cI2	3.326	—	—	—	0
		3.30[b]	—	—	—	—

[a] Exp., see Kittel [17].
[b] LDA/GGA FP-LAPW [18].
[c] LDA [19].
[d] Exp. [20].
[e] PW91, QE [9].
[f] Exp. [21].
[g] Exp. [15].
[h] PBE, CASTEP [22].
[i] PBE, ABINIT [23].

where $z = 0.4216$. We chose to remove one C atom in each sub-lattice. Optimized values are in excellent agreement with values proposed by Yvon and Parth [16]: 0.1250, 0.2917 and 0.4166, respectively.

The last system, Nb_6C_5-mC22, has a monoclinic symmetry ($C2/m$, space group *12*): C atoms are located in *2d* $(0, 1/2, 1/2)$, *4g* $(0, y = 0.3350, 0)$ and *4h* $(0, y = 0.1664, 1/2)$ and the Nb atoms are in *4i* $(x = 0.2550, 0, z = 0.7368)$ and *8j* $(x = 0.2419, y = 0.6710, z = 0.7468)$.

Finally, we considered another hexagonal phase, NbC-hP12, based on the CMo structure ($P6_3/mmc$, *194*), where C atoms are in *2a* $(0, 0, 0)$ and *4f* $(1/3, 2/3, z)$, while Nb are on the *2b* $(0, 0, 1/4)$ and *4f* sub-lattices. Our optimized values of z coordinates are 0.6650 and 0.0837, respectively.

The DFT formation energies (E_f) and lattice parameters of all structures are listed in table 1. Experimental and theoretical data are also reported for comparison. To compute the formation energies, we used carbon diamond and Nb-bcc as reference states. In the following, Ti-hcp, W-bcc and Mo-bcc were likewise used as the reference states of corresponding carbides. The carbon diamond phase was chosen instead of graphite (as is often the case in the theoretical literature) to reduce errors in the formation energy due to the Van-der-Waals interactions in the graphite, which are not taken into account in the PBE functional. This can explain the small difference between the formation energies we found and those of Hugosson [19], the difference in energy between carbon diamond and graphite is $\Delta E \simeq 15$ meV.

The formation energies of Nb–C systems agree with earlier calculations [22–24] (from 1% to 10% depending on the system and the code). All systems are non-magnetic and highly stable thermodynamically ($E_f < 0$). The most stable structure is Nb_6C_5, its formation energy is significantly lower than others, ~ -611 meV atom^{-1}.

Table 2. The formation energies (E_f, measured in meV atom^{-1}), the lattice parameters of C–Ti alloys (measured in Å), comparison with experimental data.

System		a_o	b_o	c_o	E_f
C	cF8	3.573	—	—	0
		3.567[a]	—	—	—
γ'-MoC	hP8	3.027	—	10.735	55
		2.932[b]	—	10.97[b]	—
γ-MoC	hP2	2.926	—	2.834	−149
		2.898[b]	—	2.809[b]	—
α-MoC	cF8	4.386	—	—	154
		4.266[b]	—	—	—
		4.366[f]	—	—	—
η-Mo_3C_2	hP10	3.055	—	14.631	−10
		3.018[c]	—	14.63[c]	—
ϵ-Mo_2C	hP9	5.243	—	4.787	−138
		5.19[d]	—	4.724[d]	—
ζ-Mo_2C	oP12	4.758	6.079	5.242	−156
		4.735[d]	6.025[d]	5.210[d]	—
		4.793[e]	6.003[e]	5.211[e]	—
Mo	cI2	3.170	—	—	0
		3.15[a]	—	—	—

[a] Exp., see Kittel [17].
[b] Exp. [29, 30].
[c] Exp. [28].
[d] Exp. [31, 32].
[e] PW91, US [33].
[f] PW91, QE [9].

These results clearly suggest that the atomic bonds between the metal and the carbon are very strong. The calculated lattice parameters reproduce accurately the experimental values. In most cases, DFT values are slightly higher than experimental values, a maximum deviation of about 1.5% was obtained. In the case of atomic optimized positions, the agreement with experimental findings [20, 21, 25] is excellent (see above).

3.2. Mo–C alloys

The second phase diagram, Mo–C, was described by Predel [26]. There are one cubic, one orthorhombic and four hexagonal structures in it.

The cubic phase, α-MoC, has the NaCl structure, described above. The orthorhombic structure, ζ-Mo_2C, is based on ζ-Fe_2N (*Pbcn*, *60*), where Mo atoms are located in the *8d* sublattice ($x = 0.2462, y = 0.0795, z = 0.8775$) and C atoms in *4c* ($0, y = 0.6230, 1/4$). Optimized atomic positions are in excellent agreement with experimental values [27] (0.25, 0.083 and 0.875 for Mo atoms, and 0.625 for carbon). The hexagonal phases are:

(i) γ'-MoC (prototype TiAs, $P6_3/mmc$, hP8, *194*): Mo atoms are in *4f* ($1/3, 2/3, z = 0.1198$) and C atoms in *2a* ($0, 0, 0$) and *2d* ($1/3, 2/3, 3/4$);

(ii) γ-MoC, which has the same structure than WC (hP2, $P\bar{6}m2$, *187*) where Mo atoms are in *1a* and C atoms in *1f* (see above);

(iii) η-Mo_3C_2 ($P6_3/mmc$, *194*). For this structure, we follow the description made by Yamaura *et al* [28]: Mo atoms are in *2b* ($0, 0, 1/4$), and *4f* ($1/3, 2/3, z = 0.0853$) and C in *2a* ($0, 0, 0$) and *4f* ($1/3, 2/3, z = 0.6744$). Several choices were possible for C atoms, we must put four C atoms in the 6 different sites, all of them were studied. After optimization, we obtained that atomic positions move little. Our atomic positions are in good agreement with experimental values given in [28];

(iv) ϵ-Mo_{2C} prototype ϵ-Fe_2N ($P\bar{3}1m$, *162*): Mo atoms are in *6k* ($x = 0.3329, 0, z = 0.2488$) and C in *1a* ($0, 0, 0$), *2d* ($1/3, 2/3, 1/2$).

Results are given in table 2. For all of structures, experimental and theoretical lattice parameters are in agreement, in the same way as for Nb–C systems (1%–3%). All structures are found to be metallic without magnetism. The formation energy is low, compared to the previous carbides, which can be explained by the strong stability of the Mo-bcc structure. We also obtained that α-MoC and γ'-MoC are energetically not stable

Table 3. The formation energies (E_f, in meV atom^{-1}), the lattice parameters of Ti–C alloys (in Å), comparison with experimental and theoretical data.

System		a_o	c_o	E_f
C	cF8	3.573	—	0
		3.567[a]	—	—
TiC	cF8	4.334	—	−877
		4.313[b]	—	—
		4.36[f]	—	—
		4.411[d]/4.367[e]	—	−849[e]
Ti_2C	cF48	8.642	—	−691
		8.6[c]	—	—
Ti	hP2	2.937	4.650	0
		2.95[a]	4.68[a]	—

[a] Exp., see Kittel [17].
[b] Exp. [35].
[c] Exp. [36].
[d] PBE [23].
[e] PBE [37].
[f] PW91, QE [9].

(+154 and +55 meV, respectively) compared to others Mo–C systems. This result should be relied to the fact that these structures are only observed at high temperatures (>2233 K) [26] and experimentally known to display a C-depleted off-stoichiometry.

3.3. Ti–C alloys

In the Ti–C phase diagram [34], there are only two intermediate structures, both with a cubic symmetry: (i) TiC-cF8 (NaCl prototype, see above) and (ii) Ti_2C-cF48 ($Ga_{33}Ge$ prototype, $Fd\bar{3}m$, 227), where C atoms are located in the *16c* sublattice (0, 0, 0) and Ti atoms in *32e* (x, x, x), with $x = 0.3688$.

The optimized lattice parameters, formation energies are summarized in table 3. As for previous systems, all compounds are metallic without magnetism. We found that the titanium–carbides are highly stable. Formation energy and lattice parameters of TiC are equivalent to the values obtained in earlier calculations [23, 37]. In the case of Ti_2C, only one experimental observation has been reported [36]. Our theoretical lattice parameters and optimized atomic positions (for Ti) are in agreement with the experimental measurements.

3.4. W–C alloys

In the last phase diagram, five structures were discovered. For a complete description of this phase diagram, we suggest reading the paper of Kurlov *et al* [38]. In the following we adopted the same classification Kurlov used.

There are one cubic structure, γ-WC, with the NaCl structure and one orthorhombic compound, β'-W_2C oP12 (ζ-Fe_2N as prototype, *Pbcn*, *60*). In β'-W_2C, observed at high temperature, C atoms are located in *4c* (0, y_c, 1/4) and W in *8d* (x_w, y_w, z_w). We obtained $y_c = 0.3782$, $x_w = 0.2551$, $y_w = 0.4190$ and $z_w = 0.1232$, in excellent agreement with experimental values [38]: 0.375, 1/4, 1/2 and 1/8, respectively.

Other structures have an hexagonal symmetry:

(i) δ-WC hP2 ($P\bar{6}m2$, *187*, see above): W atoms are in *1a* (0, 0, 0) and C atoms in *1f* (2/3, 1/3, 1/2). Kurlov [38] found that it is a para-magnetic structure;

(ii) β''-W_2C hP3 (CdI_2 prototype, $P\bar{3}m1$, *164*) where W atoms are in *2d* (1/3, 2/3, z) and C in *1a* (0, 0, 0). We found $z = 0.2539$ for an experimental value of 1/4;

(iii) β-W_2C hP3 ($NbZr_2$ prototype, $P6_3/mmc$, *194*): W atoms are located in *2c* (1/3, 2/3, 1/4) and one carbon in *2a* (0, 0, 0), there is a random arrangement of carbon atoms and vacancies. We choose to put a vacancy in (0, 0, 1/2). After atomic relaxation, atoms move slightly from the ideal position. These two last structures are strongly similar: when W atoms are moving along the z direction, $\beta \Longrightarrow \beta''$. In our simulations, since half of the *2a* sublattice of β-W_2C is filled with a vacancy, the final-relaxed configuration is the same as β''. Both results are thus almost the same. The difference with experimental lattice parameters can be explained either by temperature effects or by the disordered arrangement of C atoms, which were not taken into account in the present work.

Table 4. The formation energies (E_f, measured in meV atom^{-1}), the lattice parameters of C–W alloys (in Å), comparison with experimental data.

System		a_o	b_o	c_o	E_f
C	cF8	3.573	—	—	0
		3.567[a]	—	—	—
δ-WC	hP2	2.930	—	2.854	−187
		2.906[b]	—	2.837[b]	—
γ-WC	cF8	4.394	—	—	263
		4.38[c]	—	—	—
		4.266/4.252[b]	—	—	—
β''-W_2C	hP3	3.070	—	4.688	10
		2.985[b]	—	4.717[b]	—
		3.060[d]	—	4.703	0
β'-W_2C	oP12	4.761	5.243	6.113	−60
		4.728[b]	5.193[b]	6.009[b]	—
		4.745[c]	5.211	6.088	−20
β-W_2C	hP3	3.070	—	4.687	10
		3.002[b]	—	4.75[b]	—
		3.19[d]	—	4.626[d]	−62[d]
W_2C	hP9	5.260	—	4.786	−44
W_2C	oP6	3.043	4.726	5.298	−55
W	cI2	3.192	—	—	0
		3.165[a]	—	—	—

[a] Exp., see Kittel [17].
[b] Exp. [38].
[c] PW91, QE [9].
[d] PW91, US [33].

In addition, two other structures were studied: (i) W_2C hP9 (ϵ-Fe_2N, $P\bar{3}1m$, *162*) where W atoms are in *6k* ($x = 0.6679, 0, z = 0.7523$) and C atoms in *1a* (0, 0, 0) and in *2d* (1/3, 2/3, 1/2) and (ii) W_2C (*Pnnm*, oP6, *58*) where W atoms in *4g* ($0, y = 0.2583, z = 0.1588$) and C atoms in *2a* (0, 0, 0).

Results are listed in table 4. As for previous phase diagrams, simulations reproduced accurately experimental lattice parameters. γ-WC and β-W_2C have positive formation energies like MoC-cF8, especially the γ phase. These structures should be stabilized thanks T. δ-WC, the more stable structure, is the only phase observed at low T (below 1500 K). The absence of magnetism is in agreement with experimental results.

4. Elastic properties

To compute elastic constants C_{ij}, we choose to use the second derivatives of the energy with respect to the atomic positions of DFT. It is convenient to represent the second-order elastic constant with a symmetric 6 × 6 matrix:

$$C_{ij} = \begin{pmatrix} C_{11} & C_{12} & C_{13} & C_{14} & C_{15} & C_{16} \\ & C_{22} & C_{23} & C_{24} & C_{25} & C_{26} \\ & & C_{33} & C_{34} & C_{35} & C_{36} \\ & & & C_{44} & C_{45} & C_{46} \\ & & & & C_{55} & C_{56} \\ & & & & & C_{66} \end{pmatrix}. \quad (1)$$

For cubic structures, there are only three independent constants, i.e., C_{11}, C_{12} and C_{44}. In the case of orthorhombic phases, there are nine constants: C_{ii}, (i = 1–6), C_{12}, C_{13} and C_{23}. For hexagonal compounds, there are five independent parameters (C_{11}, C_{33}, C_{12}, C_{13} and C_{44}). Other parameters (also computed) are linked to each others: $C_{11} = C_{22}$, $C_{12} = C_{13}$, $C_{44} = C_{55}$, and $C_{66} = (C_{11} - C_{12})/2$.

Table 5 summarizes the calculated elastic constants of all carbides and reference states. In addition to the elastic constants, we report the bulk (B_H), the Young (E) and the shear moduli (G_H), the Poisson' ratio (ν), and the Debye temperatures (Θ_D).

For the reference states (Ni, Nb, Ti, Mo, W and C), DFT simulations lead to excellent results when compared to experimental values [17, 42]. The discrepancy is low, <5% for most elastic constants. The principal differences concern the C_{44} values, for which we obtain in the case of Mo a lower value, the difference is of 40% for an unexplained reason. On the contrary, in the case of Nb, Ti, C and Ni, simulations reproduce accurately

Table 5. Elastic constants C_{ij} (in GPa), bulk modulus (B_H, in GPa), Young modulus E (in GPa), Hill shear modulus (G_H, in GPa), the Poisson ratio ν, and the Debye' temperature Θ_D (in K) of carbides, comparison with the reference states and theoretical literature. As an additional information, we also give the ratio bulk to shear modulus. The last column gives the vibrational enthalpy at 0K (ZPE, in meV atom^{-1}.)

	C_{11}	C_{22}	C_{33}	C_{12}	C_{23}	C_{13}	C_{44}	C_{55}	C_{66}	B_H	G_H	B_H/G_H	E	ν	Θ_D	ZPE
Ni-cF4	246[a]	—	—	165	—	—	108	—	—	191	73	2.62	194	0.33	433	35
	250[b]	—	—	150	—	—	131	—	—	183	98	—	230	0.29	450	—
C-cF8	1045[a]	—	—	124	—	—	558	—	—	430	517	0.83	1108	0.07	2210	173
	1076[c]	—	—	125	—	—	576	—	—	442	535	—	1141	0.07	2230	—
NbC-cF8	626[a]	—	—	130	—	—	163	—	—	295	192	1.53	474	0.23	739	−33
	620[l]	—	—	127	—	—	161	—	—	294	193	—	475	—	—	—
	630[m]	—	—	200	—	—	150	—	—	296	200	—	494	—	—	—
NbC-hP12	530[a]	—	515	168	184	—	120	—	181	293	151	1.95	387	0.28	658	−33
NbC-hP2	449[a]	—	673	164	132	—	39	—	142	266	96	2.77	257	0.34	532	−42
Nb_4C_3-hR20	440[a]	—	397	153	155	—	91	—	144	244	116	2.09	302	0.29	560	—
Nb_6C_5-mC22	417[a,e]	432	428	124	148	131	171	183	158	231	158	1.46	386	0.22	656	−25
β-Nb_2C-hP9	400[a,f]	—	410	164	152	—	121	—	118	238	120	1.98	309	0.28	544	−16
γ-Nb_2C-hP3	396[a,g]	—	411	144	119	—	38	—	126	218	50	4.30	141	0.39	359	−16
Nb_2C-oP12	423[a]	400	412	118	141	132	129	113	78	223	117	1.91	299	0.28	537	−15
Nb-cI2	251[a]	—	—	131	—	—	26	—	—	171	36	4.66	102	0.40	268	25
	236[b]	—	—	139	—	—	29	—	—	171	40	—	103	0.40	275	—
C-cF8	1045[a]	—	—	124	—	—	558	—	—	430	517	0.83	1108	0.07	2210	173
	1076[c]	—	—	125	—	—	576	—	—	442	535	—	1141	0.07	2230	—
TiC-cF8	511[a]	—	—	125	—	—	162	—	—	253	174	1.46	425	0.22	908	−12
	457	—	—	113	—	—	169	—	—	227	170	—	408	—	—	—
	500[a]	—	—	112	—	—	175	—	—	240	187	—	450	—	—	—
Ti_2C-cF48	203[a]	—	—	110	—	—	114	—	—	141	79	1.77	201	0.26	590	−24
Ti-hP2	173[a]	—	178	85	79	—	42	—	44	112	44	2.54	117	0.33	402	32
	160[c]	—	181	90	66	—	46	—	35	105	44	—	116	0.33	420	—
C-cF8	1045[a]	—	—	124	—	—	558	—	—	430	517	0.83	1108	0.07	2210	173
	1076[c]	—	—	125	—	—	576	—	—	442	535	—	1141	0.07	2230	—
δ-WC-hP2	672[a]	—	929	246	169	—	293	293	213	380	267	1.42	649	0.22	627	−52
γ-WC-cF8	648[a]	—	—	220	—	—	103	—	—	362	138	2.62	368	0.33	457	−32
β''-W_2C-hP3	503[a,h]	—	509	161	240	—	168	—	171	309	156	1.98	401	0.28	437	−30
β'-W_2C-oP12	513[a]	540	534	263	186	251	166	205	192	331	168	1.96	433	0.28	454	−28
β-W_2C-hP3	505[a,i]	—	528	148	243	—	171	—	179	309	161	1.92	412	0.28	444	−30
W_2C-hP9	522[a,j]	—	494	201	263	—	198	—	161	332	161	2.06	416	0.29	444	−28

Table 5. (Continued.)

	C_{11}	C_{22}	C_{33}	C_{12}	C_{23}	C_{13}	C_{44}	C_{55}	C_{66}	B_H	G_H	B_H/G_H	E	ν	Θ_D	ZPE
W_2C-oP6	532[a]	523	549	244	258	186	224	172	169	330	171	1.93	437	0.28	457	−28
W-cI2	538[a]	—	—	186	—	—	150	—	—	303	160	1.90	408	0.28	382	39
	532[b]	—	—	205	—	—	164	—	—	314	163	—	417	0.28	400	—
C-cF8	1045[a]	—	—	124	—	—	558	—	—	430	517	0.83	1108	0.07	2210	173
	1076[c]	—	—	125	—	—	576	—	—	442	535	—	1141	0.07	2230	—
γ'-MoC-hP8	499[a]	—	486	150	302	—	149	—	175	327	134	2.44	354	0.32	605	−43
γ-MoC-hP2	613[a]	—	836	206	170	—	252	—	204	348	239	1.45	584	0.22	800	−27
α-MoC-cF8	649[a]	—	—	174	—	—	108	—	—	332	148	2.23	388	0.31	637	−49
η-Mo_3C_2-hP10	472[a]	—	469	178	187	—	101	—	147	279	124	2.24	326	0.31	551	−32
ϵ-Mo_2C-hP9	480[a,k]	—	448	180	219	—	169	—	150	293	148	1.98	380	0.28	581	−22
ζ-Mo_2C-oP12	454[a]	487	490	224	166	212	146	184	171	292	153	1.91	391	0.28	590	−21
Mo-cI2	453[a]	—	—	161	—	—	74	—	—	257	97	2.64	260	0.33	416	34
	450[n]	—	—	173	—	—	125	—	—	265	130	—	335	0.29	450	—

[a] PBE, VASP present work.
[b] PBE, VASP/Exp., see [39].
[c] Exp., see [40].
[d] $C_{15} = 1, C_{25} = -1$ and $C_{46} = -1$.
[e] We also found −23, 26, 26 and 0.3 for C_{ij} where ij = 16, 26, 45 and 36, respectively.
[f] $C_{16} = 16, C_{26} = -16$ and $C_{46} = -16$.
[g] $C_{15} = 48, C_{25} = -48$ and $C_{56} = 48$.
[h] $C_{15} = 30, C_{25} = -30$ and $C_{46} = 30$.
[i] $C_{15} = 24, C_{25} = -24$ and $C_{46} = 24$.
[j] $C_{16} = -8, C_{26} = 8$ and $C_{45} = 8$.
[k] $C_{16} = 5, C_{26} = -5$ and $C_{45} = 5$.
[l] Exp., ABINIT from Hua *et al* [23].
[m] Exp. [41].
[n] Exp. [42].

experimental data. With reference to carbides, only cF8 elastic properties have been investigated theoretically. For example, Isaev [9] only reported bulk modulus for cF8 structures (242, 301, 337 and 365 GPa for TiC, NbC, MoC and WC respectively, to compare to our values: 253, 295, 332 and 362GPa), and Hua *et al* [23] related a whole set of elastic constants (see C_{ij} listed in table 4). Calculated with different methods, the discrepancy between theoretical values is low, approximately 1%–3%. We also note the excellent agreement with experimental values [41].

From these constants, additional properties were investigated: (i) the elastic stability, (ii) the polycrystalline properties and (iii) the Debye temperature.

Using relations established by Mouhat [43], we first verified that criteria for mechanical stability were met for all structures, which is consistent with experiments.

From elastic constants, polycrystalline properties were then computed: the Young, bulk and shear modulis, using the Reuss and Voigt approximation. In the case of cubic phases, the bulk modulus B is given by $B = (C_{11} + 2C_{12})/3$ (the Voigt and Reuss approximations give the same value), while the Voigt and Reuss shear modulus G (G_v and G_r, respectively) are equal to:

$$\begin{cases} 5G_v = (C_{11} - C_{12}) + 3C_{44}, \\ 5/G_r = 4(S_{11} - S_{12}) + 3S_{44}, \end{cases} \tag{2}$$

where S_{ij} ($i, j \in [1, 3]$) is the compliance matrix, given by $\mathbf{S} = \mathbf{C}^{-1}$. The mean Poisson' ratio (ν) is thus given by:

$$\nu = \frac{1}{2}\left[\frac{3B - 2G}{3B + G}\right] \tag{3}$$

and the Young modulus E:

$$E = \frac{9GB}{3B + G}, \tag{4}$$

where G and B are mean values of the shear and bulk moduli. More general relationships for $G_{v,r}$ and $B_{v,r}$ exist for all Bravais lattices [44]:

$$\begin{cases} B_v = \frac{1}{9}(C_{11} + C_{22} + C_{33} + 2(C_{12} + C_{13} + C_{23}) \\ \frac{1}{B_r} = S_{11} + S_{22} + S_{33} + 2(S_{12} + S_{13} + S_{23}) \end{cases} \tag{5}$$

and

$$\begin{cases} 15G_v = \sum_i C_{ii} - (C_{12} + C_{23} + C_{31}), \\ \frac{15}{G_r} = 4\sum_i S_{ii} - 4(S_{12} + S_{23} + S_{31}) - (S_{44} + S_{55} + S_{66}). \end{cases} \tag{6}$$

The mean bulk and shear moduli as a function of C content are plotted in figure 1. One can note that no general trend can be extracted from our results. For instance, the bulk modulus varies almost linearly with carbon concentration, contrary to the shear and Young moduli. This trend can be explained by the covalent nature of the bonds when the number of C atoms increases. The ratio of bulk to shear modulus, B/G, was proposed by Pugh [45] as an indicator criteria of ductile versus brittle characters. The shear modulus G represents the resistance to a plastic deformation, while the bulk modulus B represents the resistance to fracture. A high B/G value suggests a tendency for ductility, while a low value indicates a tendency for brittleness. The transition value, which separates ductile and brittle behaviors, was evaluated to be equal to about 1.75, based on experimental data. This ratio, reported in table 5, allow to predict that only four compounds should have a brittle behavior (hP2 structure for WC and MoC, and cF8 for NbC and TiC), the others should be ductile. There no common feature between the structure and brittle/ductile behavior.

To conclude, we compute the Debye temperature, Θ_D, by means of the following relation:

$$\Theta_D = \frac{h}{k_B}\left(\frac{3}{4\pi V_a}\right)^{1/3} \nu_m, \tag{7}$$

where ν_m is the average sound velocity in polycrystals, V_a the atomic volume. ν_m was calculated with:

$$\frac{1}{\nu_m^3} = \frac{1}{3}\left(\frac{2}{\nu_t^3} + \frac{1}{\nu_l^3}\right), \tag{8}$$

where ν_l and ν_t, the mean longitudinal and transverse sound velocities, are related to elastic constants by the shear and bulk moduli and the density ρ:

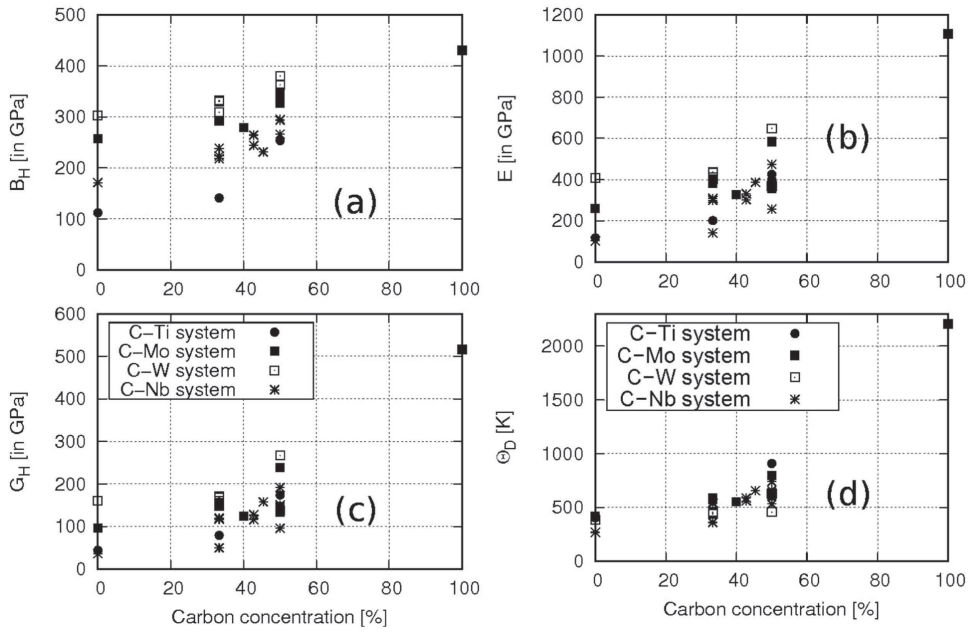

Figure 1. Bulk (a), Young (b) and shear (c) moduli and Debye temperature (d) as a function of C content.

$$3\rho v_l^2 = 3B + 4G \text{ and } \rho v_t^2 = G. \tag{9}$$

There is little data on this matter in the literature. Smith [7] summarized experimental values regarding NbC-cF8 and β-Nb_2C. In the first system, the experimental value, which was measured between 446 and 500 K, is in good agreement with our theoretical value (473 K). In the case of β-Nb_2C, we obtained a value of 544 K, that falls within the experimental interval of [460; 660] K. Our results are shown in figure 1. In the case of tungsten carbides, Θ_D is almost constant, while in molybdenum systems, there is a strong variation (416–800 K). It is noticeable that high values always correspond to brittle systems (NbC-cF8, TiC-cF8, δ-WC and γ'-MoC).

5. Vibrational properties

Finally, we computed the vibration properties using the finite displacements approach (frozen-phonon approach). From the forces calculated with a reduced number of finite displacements, we deduced IFCs. By sampling the dynamical matrix for wave vectors, we calculate the vibrational density of states (total and projected density of states on non-equivalent atoms are represented) on fine q-meshes grids and plotted the dispersion curves. Results are depicted on figures 2–5.

From vibrational projected density-of-states, we deduced that motions within acoustic dispersion curves are thus almost entirely due to transition metal atoms and that optic modes correspond to the vibration of the C atoms. Carbon frequencies are thus almost always significantly higher in energy than those of the transition metals, inducing a wide gap (forbidden band) in the vibrational structures. The width of this gap results from the great mass difference between C atoms and the transition metals (4–12 times lighter). The dispersion curves around the Γ point (associated to the sound waves) do not show any anomaly, which is in agreement with our results on the mechanical criteria.

Here, again, experimental data are lacking, most results (experimental and theoretical studies) concern only cubic structures. For instance, in the case of cF8 structures, the comparison with frequencies computed by Isaev is excellent. The discrepancy in frequencies is less than 1% for TiC, 1%–4% for NbC. The finite displacement method and density functional perturbative theory (DFPT), used by Isaev [9], therefore provide similar results. The comparison with experimental TiC density of states reported by Pintschovius [46] is excellent, this further validates other results.

Two structures have imaginary frequencies: α-MoC and β-WC. In their work on cubic mono-carbides, Isaev *et al* [9] also note that α-MoC and β-WC show many imaginary frequencies. These structures are dynamically unstable, despite the fact that they are mechanically stable. These results are confirmed when we increase significantly the size of the super-cells used to compute IFC ($3 \times 3 \times 3$ super-cells, i.e., 216 atoms per cell). In the phase diagram, these structures are not stoichiometric: the carbon concentration is off-stoichiometric ($C_{1-x}W$ and C_{1-x} Mo, see the phase diagrams [38] and [26], respectively) and they are

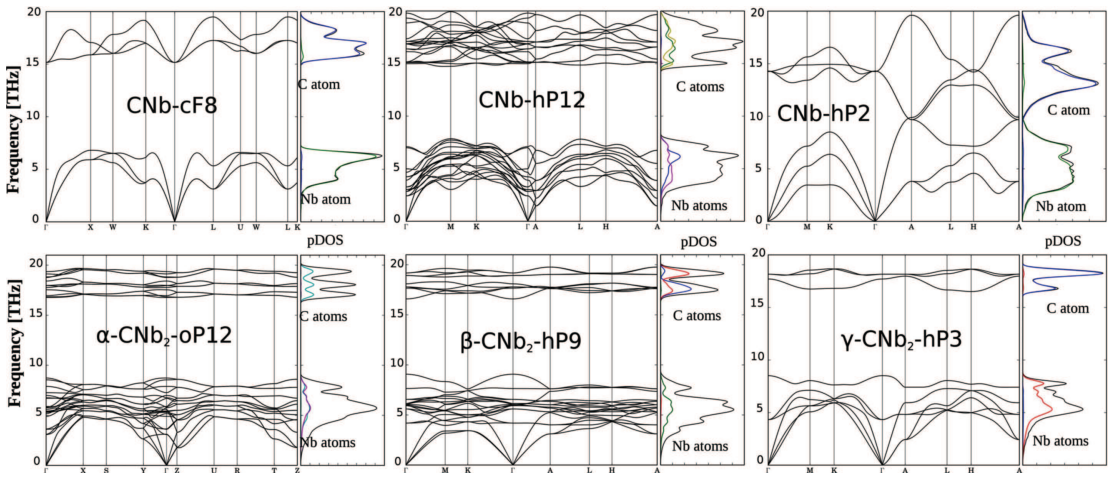

Figure 2. Vibrational band structures and total density of states (in black) of Nb–C structures, frequencies are in THz. Band structures are plotted along high symmetry points of the first Brillouin zones. The projected density of states on non-equivalent species is also represented.

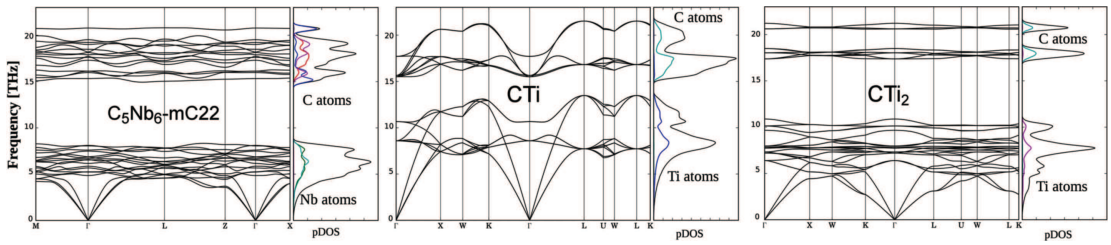

Figure 3. Vibrational band structures and density of states (in black) of Nb_6C_5, TiC and Ti_2C, frequencies are in THz. For TiC, we did not use the primitive cell, we used the cubic structure (8 atoms per lattice).

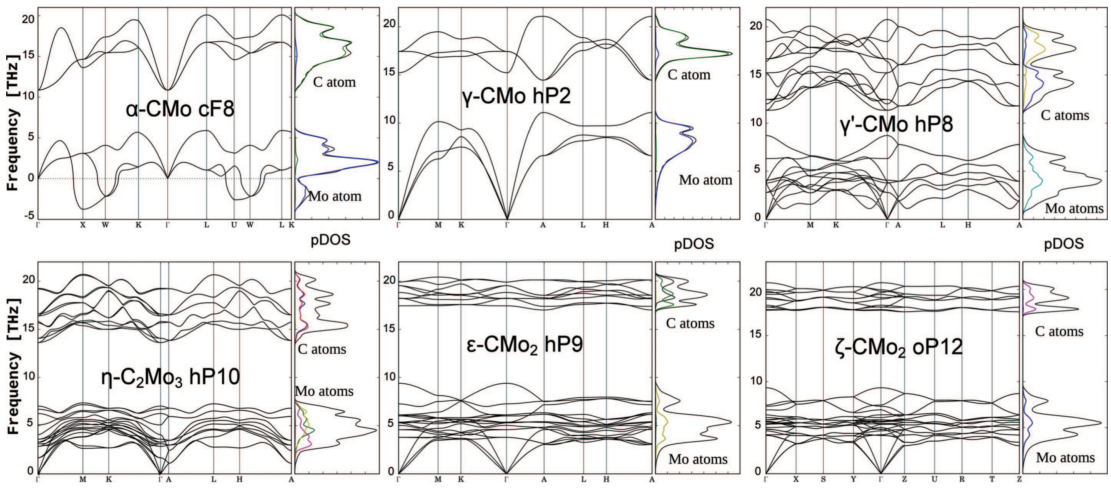

Figure 4. Vibrational band structures and density of states of α-, γ- and γ'-MoC, η-Mo_3C_2 and ϵ- and ζ-Mo_2C, frequencies are in THz.

synthesized only at high temperatures. Thermal effects and intrinsic defects could explain the stability of these structures.

We sought a trend concerning vibrational properties. For identical structures, vibrational properties are quite similar: hP9 (β-Nb_2C, ϵ-Mo_2C and W_2C), hP2 (γ-WC, γ-MoC, NbC), oP12 (Nb_2C, ζ-Mo_2C and β'-W_2C), cF8 structures and hP3 (β-W_2C and γ-Nb_2C) structures. The difference between Nb, W, Mo systems can be rationalized using their respective atomic weights.

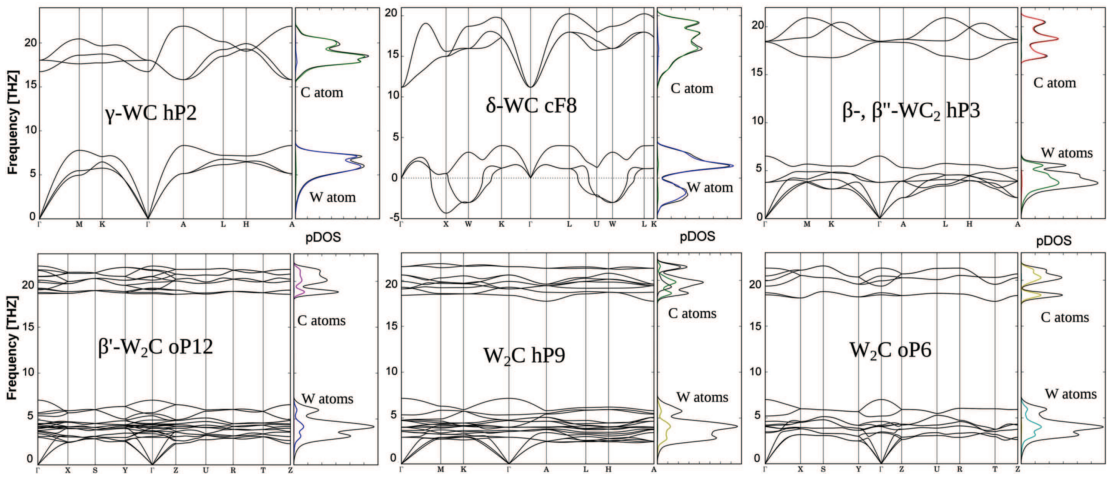

Figure 5. Vibrational band structures and density of states of γ- and δ-WC and β''-, β'- and β-W_2C, frequencies are in THz.

Finally, from the vibrational properties, the zero-point energy (ZPE) of all structures were computed at 0K (see last column in table 5). Enthalpy energy is slightly lower of about 20–40 meV, that which does not change the relative stability of the phases.

6. Conclusion

We have used first-principles calculation for a complete and systematic study of transition metal carbides alloys. DFT results of the ground state properties yield excellent agreement with experimental measurements and observations. The theory reproduce accurately lattice parameters and atomic positions of structures. From elastic constants, we deduce that all structures are mechanically stable. However, from vibrational dispersion curves, we obtain that some structures should not be stable at low temperature.

Acknowledgments

This work was granted access to the HPC resources of CALMIP (CICT Toulouse, France) under the allocation 2016-p0749 and 2016-p0842. Author thanks J Huez and B Malard for fruitful discussions.

References

[1] Ivashchenko V I, Turchi P E A and Olifan E I 2010 Phase stability and mechanical properties of niobium nitrides *Phys. Rev.* B **82** 054109
[2] Holec D, Friák M, Neugebauer J and Mayrhofer P H 2012 Trends in the elastic response of binary early transition metal nitrides *Phys. Rev.* B **85** 064101
[3] Brik M and Ma C-G 2012 First-principles studies of the electronic and elastic properties of metal nitrides {*X*N} (*X* = Sc, Ti, V, Cr, Zr, Nb) *Comput. Mater. Sci.* **51** 380–8
[4] Sims C T 1984 A history of superalloy metallurgy for superalloy metallurgists *Proc. Superalloys 1984 (TMS)* ed E A Loria p 399
[5] Sabol G and Stickler R 1969 Microstructure of nickel-based superalloys-review article *Phys. Status Solidi* **39** 11
[6] Jena A and Chaturvedi M 1984 The role of alloying elements in the design of nickel-base superalloys *J. Mater. Sci.* **19** 3121
[7] Smith G D and Patel S J 2005 The role of niobium in wrought precipitation-hardened nickel-base alloys *Proc. Superalloys 718, 625, 706 and Various Derivatives (TMS)* ed E A Loria p 135
[8] Singleton M and Nash P 1989 The C–Ni (carbon–nickel) system *Bull. Alloy Phase Diagr.* **10** 121–6
[9] Isaev E I, Simak S I, Abrikosov I A, Ahuja R, Vekilov Y K, Katsnelson M I, Lichtenstein A I and Johansson B 2007 Phonon related properties of transition metals, their carbides, and nitrides: a first-principles study *J. Appl. Phys.* **101** 123519
[10] Kresse G and Hafner J 1993 *Ab initio* molecular dynamics for liquid metals *Phys. Rev.* B **47** 558R
[11] Kresse G and Joubert D 1999 From ultrasoft pseudopotentials to the projector augmented-wave method *Phys. Rev.* B **59** 1758
[12] Perdew J, Burke K and Ernzerhof M 1997 Generalized gradient approximation made simple *Phys. Rev. Lett.* **78** 1396
[13] Le Page Y and Saxe P 2002 Symmetry-general least-squares extraction of elastic data for strained materials from *ab initio* calculations of stress *Phys. Rev.* B **65** 104104
[14] Togo A, Oba F and Tanaka I 2008 First-principles calculations of the ferroelastic transition between rutile-type and Ca *Phys. Rev.* B **78** 134106
[15] Smith J F, Carlson O N and DeAvillez R R 1987 The niobium–carbon system *J. Nucl. Mat.* **148** 1
[16] Yvon K and Parthé E 1970 On the crystal chemistry of the close-packed transition-metal carbides: I. The crystal structure of the ζ-V, Nb and Ta carbides *Acta Crystallogr.* B **26** 149–53
[17] Kittel C 1996 *Introduction to Solid State Physics* (New York: Wiley)

[18] Amriou T, Bouhafs B, Aourag H, Khelifa B, Bresson S and Mathieu C 2003 FP-LAPW investigations of electronic structure and bonding mechanism of NbC and NbN compounds *Physica* B **325** 46
[19] Hugosson H, Eriksson O, Jansson U and Johansson B 2001 *Phys. Rev.* B **63** 134108
[20] Rudy E, Benesovsky F and Toth L 1963 *Z. Met. k.d.* **54** 345
[21] Khaenko B and Sivak O 1989 *Dopov. Akad. Nauk Ukr. RSR* A **51** 78
[22] Wu L, Wang Y, Yan Z, Zhang J, Xiao F and Liao B 2013 The phase stability and mechanical properties of Nb–C system: using first-principles calculations and nano-indentation *J. Alloys Compd.* **561** 220–7
[23] Hua G and Li D 2015 A first-principles study on the mechanical and thermodynamic properties of (Nb1-xTix)c complex carbides based on virtual crystal approximation *RSC Adv.* **5** 103686–94
[24] Zaoui A, Kacimi S, Bouhafs B and Roula A 2005 First-principles study of bonding mechanisms in the series of Ti, V, Cr, Mo, and their carbides and nitrides *Physica* B **358** 63–71
[25] Zubkov V, Dubrovskaya L, Gel'd P, Ckhaj V and Dorofeev Y 1969 *Dokl. Akad. Nauk SSSR* **184** 874
[26] Predel B 1992 C–Mo (Carbon–Molybdenum) *B-Ba—C-Zr* (Berlin: Springer) pp 1–4
[27] Parthé E and Sadogopan V 1963 The structure of dimolybdenum carbide by neutron diffraction technique *Acta Crystallogr.* **16** 202–5
[28] Yamaura K, Huang Q, Akaishi M and Takayama-Muromachi E 2006 Superconductivity in the hexagonal-layered molybdenum carbide η-Mo_3C_2 *Phys. Rev.* B **74** 184510
[29] Kuo K and Hägg G 1952 *Nature* **170** 245
[30] Clougherty E, Lothrop K and Kafalas J 1961 *Nature* **191** 1194
[31] Rudy E, Windisch S, Stosick A and Hoffman J 1967 *Trans. AIME* **239** 1247
[32] Epicier T, Dubois J, Esnouf C, Fantozzi G and Convert P 1988 *Acta Metal.* **36** 1903
[33] Abderrahim F, Faraoun H and Ouahrani T 2012 Structure, bonding and stability of semi-carbides {M2C} and sub-carbides {M4C} (M =V, Cr, Nb, Mo, Ta, W): a first principles investigation *Physica* B **407** 3833–8
[34] Murray J and Wriedt H 1987 *Phase Diagrams of Binary Titanium Alloy* (New York: ASM)
[35] Ehrlich P and Anorg Z 1949 *Z. Anorg. Chem.* **259** 1
[36] Goretzki H 1967 *Phys. Status Solidi* **20** K141
[37] Jang J H, Lee C-H, Heo Y-U and Suh D-W 2012 Stability of (Ti, M)C (M = Nb, V, Mo and W) carbide in steels using first-principles calculations *Acta Mater.* **60** 208–17
[38] Kurlov A S and Gusev A I 2005 Tungsten carbides and W–C phase diagram *Inorg. Mater.* **42** 121–7
[39] Connétable D, Mathon M and Lacaze J 2011 First principle calculations of Fe–Nb–Ni–Cr systems *Calphad, Comput. Coupling Phase Diagr. Thermochem.* **35** 588
[40] Connétable D 2010 *Phys. Rev.* B **82** 075209
[41] Weber W 1973 *Phys. Rev.* B **8** 5082–92
[42] Featherston F H and Neighbours J R 1963 Elastic constants of tantalum, tungsten, and molybdenum *Phys. Rev.* **130** 1324–33
[43] Mouhat F and Coudert F M C-X 2014 Necessary and sufficient elastic stability conditions in various crystal systems *Phys. Rev.* B **90** 224104
[44] Hill R 1952 The elastic behaviour of a crystalline aggregate *Proc. Phys. Soc.* A **65** 349
[45] Pugh S 1954 XCII. Relations between the elastic moduli and the plastic properties of polycrystalline pure metals *Phil. Mag. Series* **7** 823–43
[46] Pintschovius L, Reichardt W and Scheerer B 1978 *J. Phys. C: Solid State Phys.* **11** 1557